Diaphragm stress analysis and fatigue strength evaluation of the flex-spline, a very thin-walled spur gear used in the strain wave gearing

Shuting Li*

Department of Mechanical, Electrical and Electronic Engineering,
Interdisciplinary Faculty of Science and Engineering,
Shimane University, Matsue, 690-8504, Japan

Abstract

This paper deals with diaphragm stress analysis and fatigue strength calculation problems of the flex-spline, a thin-walled spur gear used in the strain wave gearing (SWG). Firstly, a mechanics model and theoretical method used for contact analysis of SWG are presented in this paper. Then finite element method (FEM) software is self-developed through a very long time efforts in order to realize the contact analysis and stress calculations of SWG. With the developed FEM software, bending and shear stresses of the diaphragm of the flex-spline are analyzed successfully. Secondly, in order to confirm the FEM software, an experimental method and device are presented in this paper. A three-directional, strain gauge is stuck on a straight surface of the tapered diaphragm of the flex-spline next to the corner of the diaphragm with the boss. Diaphragm strains are measured under the conditions of zero and 110Nm torques respectively and the measured stresses are compared with the calculated ones with the developed FEM software under the same conditions. It is found that the two results are in agreement with each other well. This means that the presented mechanics model and theoretical method are correct and effective. Finally, a method used to evaluate fatigue failure strength of the diaphragm is suggested based on the findings in this paper.

1. Introduction

The strain wave gearing (SWG), often called the harmonic drive device, is a gear reducer with many advantages, such as lightweight, small size, high speed ratio, low backlash et al. So, it is widely used in industrial robots (as joints), semi-conductor devices and space-exploring machines et al. Though so many units of this gear reducer are used in industry, strength calculation problems of this gear device have not been solved completely since its invention in 1959 [1-2]. This is because elastic deflection of the flex-spline, a very thin-walled spur gear, is used to generate tooth engagement movement, a completely different type of tooth engagement movement from other gears such as spur gears.

Shen [3] and Nbahob [4] studied strength calculation problems of the tooth root of SWG. Alfutov [5] and Le [6-7] studied tooth load calculation problems of SWG using a method of material mechanics. Cui [8] studied tooth load analysis and root stress calculations of SWG using a two-dimensional (2D), FEM. Ishida [9] and Sentoku [10] studied tooth load distribution evaluation using an experimental method. Some recent papers on SWG and static load sharing in internal involute spur gearing with thin rimmed pinion can also be found in the studies of Maiti et al [11-12]. Though so many papers can be found, diaphragm stress analysis and fatigue strength calculation problems of the flex-spline could not be investigated in these papers.

Li [13-14] also studied strength calculation problems of SWG. Though the phenomenon of fatigue breakage failure of the diaphragm was introduced in Li's research, problems of stress analysis and fatigue strength calculation of the diaphragm could not be investigated deeply. The reality is that the problems of stress analysis and fatigue strength calculation of the diaphragm are still remained as unsolved problems. This paper tries to solve the problems completely.

Breakage at the corner of the diaphragm with the boss of the flex-spline is a typical fatigue failure pattern of SWG. In order to avoid this breakage, it is necessary to find the reasons why the breakage happened at the corner. Also, it is necessary to find a suitable method that can calculate stress levels of the corner and evaluate fatigue failure strength of the corner. To realize this aim, this paper presents a mechanics model and principle used for contact analysis of SWG based on the mathematical programming method [15-16]. Special FEM software development is conducted to realize the aim through a very long time effort. With the self-developed FEM software, it becomes possible to analyze diaphragm stress calculations of the flex-spline. An experimental method and device are also presented in the paper to confirm the mechanics model and principle presented in this paper. It is found that the calculation results are in agreement with the experiment ones well. This means that the mechanics model and method presented in this paper are reasonable. Finally, it is suggested that the maximum shear stress at the corner should be used to evaluate fatigue strength of the diaphragm.

* Tel./fax: +81 0852 328908.

E-mail address: shutingli@ecs.shimane-u.ac.jp

2. Structure of SWG

Figure 1 is a so-called cup-type of SWG. It mainly consists of four components: (1) the flex-spline (FS), an very thin-walled spur gear taking the shape of a cup; (2) the circular spline (CS), an internal spur gear; (3) the wave generator (WG), an elliptical cam that can change the shape of FS from a round shape into an elliptical one; (4) the flexible ball bearing (FB), a thin-walled ball bearing mounted on the outside of WG. Since walls of the outer and inner rings are very thin, this bearing can be deformed very easily by WG. FS is deformed by WG with FB when WG with FB is inserted into FS at the working state.

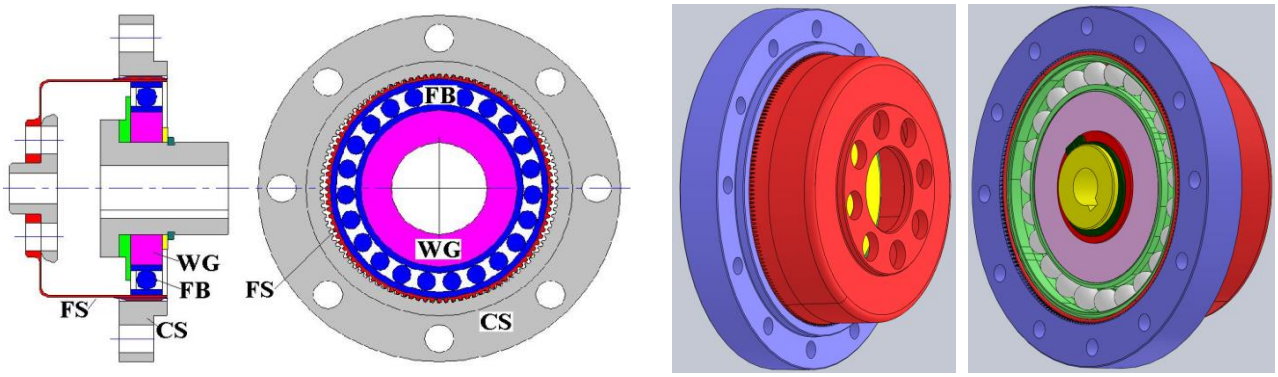

Fig.1 Main structure of a strain wave gearing

3. Fatigue breakage failure of the diaphragm at the corner

Figure 2 is a section drawing of FS structure with fatigue breakage at the corner (the joint) of the diaphragm with the boss. As shown in Fig.2, the diaphragm has the fatigue breakage at the part of stress concentration of FS structure. This failure pattern is very dangerous for industrial robots when SWG is used as joints. So, it is necessary to avoid this fatigue failure in the stage of designing SWG.

In order to avoid the fatigue breakage of the diaphragm, it is necessary to know the position of the maximum stress point at the corner at the first. Also it is necessary to find a suitable method that can calculate the diaphragm stresses of the corner correctly. But since FS is a very thin-walled spur gear and the gearing principle of SWG is completely different from usual gears, the problems of diaphragm stress analysis and strength calculation have not been solved so far. This paper attempts to solve it completely through a more than 20 years' preparation of the author.

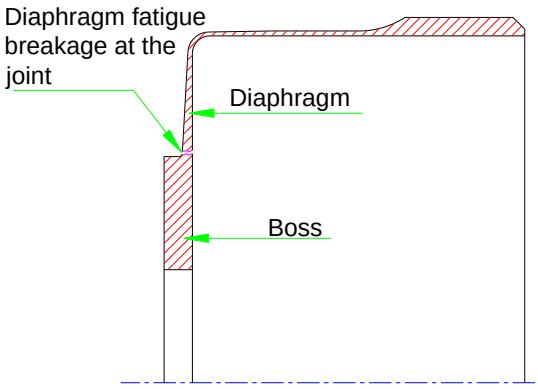

Fig.2 Fatigue breakage of FS at the corner of the diaphragm with the boss

4. Experimental investigations on the diaphragm stresses

4.1 SWG used as research object

CSF40-100 made by Harmonic Drive Systems Inc. [17] is purchased and used as research object in this paper. Speed ratio and rated torque of this SWG are $i = 100$ and T =265Nm respectively. The main structural dimensions of this SWG can be available through the homepage of the maker. Other dimensions and gearing parameters of this SWG that cannot be available from the maker are measured and guessed using the purchased CSF40-100. Since it is still a trade secret for the maker, design parameters of CSF40-100 are not shown in this paper. Figure 3 is a photo of WG, FS and CS of CSF40-100.

Fig. 3 WG, FS and CS of CSF40-100 (from the left to right)

4.2 Experimental device, methods and conditions

An experimental device as shown in Fig.4 is presented to do experimental research on diaphragm stress measurements in order to confirm the results obtained by the theoretical analysis. This device consists of (1) an induction motor with no-step speed reducer (NIDEC-SHIMPO, RXM-200B), used to offer power and variable low speed for SWG; (2) parts used to fix FS, CS and WG; (3) a torque meter (Kyowa, TP-50KMCB) used to measure torque load; (4) a powder brake (Mitsubishi, ZKB-20XN) used to provide torque load for SWG.

In Fig.4, in order to measure and output strain signals easily from the diaphragm when FS is running, the diaphragm of FS is open to the outside. So, if FS runs at a very low speed (about 3 to 5min^{-1}), the measurement can be realized. It is not worried that signal cables of strain gauges get entangled on the surfaces of FS and other rotating parts. Measured diaphragm strain signals are sent into a data recorder called EDS400 (Kyowa) as shown in Figs. 4 and 5 through three bridge boxes (Kyowa). EDS400 has three functions: (1) Dynamic strain amplifier; (2) A/D conversion; (3) Data sampling. A personal computer is connected to EDS400 by a LAN cable to realize the three functions using special software developed by the maker. Fig.5 is a photo of the experimental device.

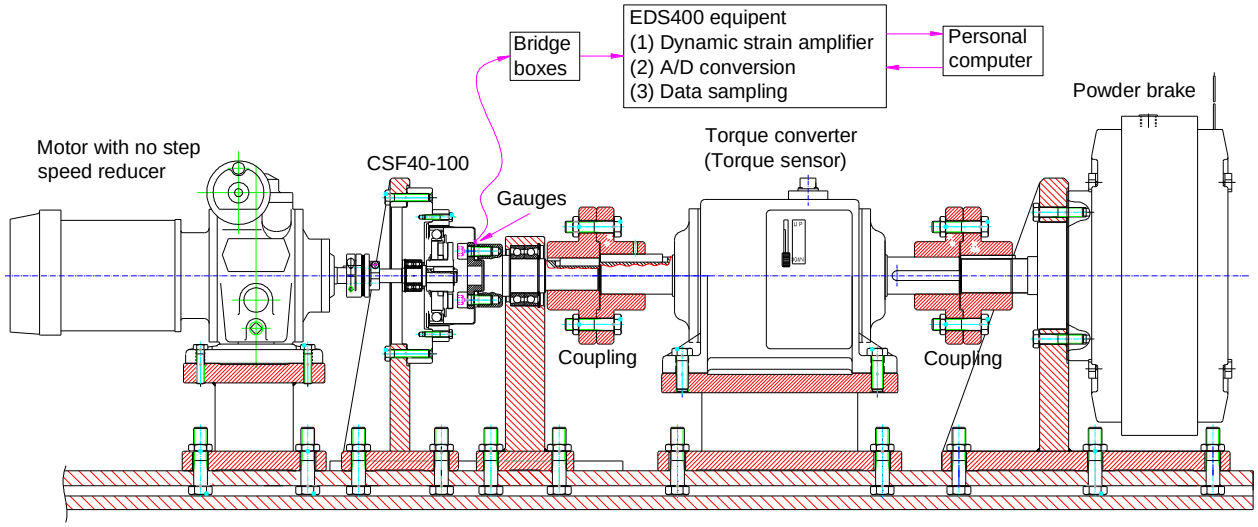

Fig.4 Experimental device used for the diaphragm strain measurement

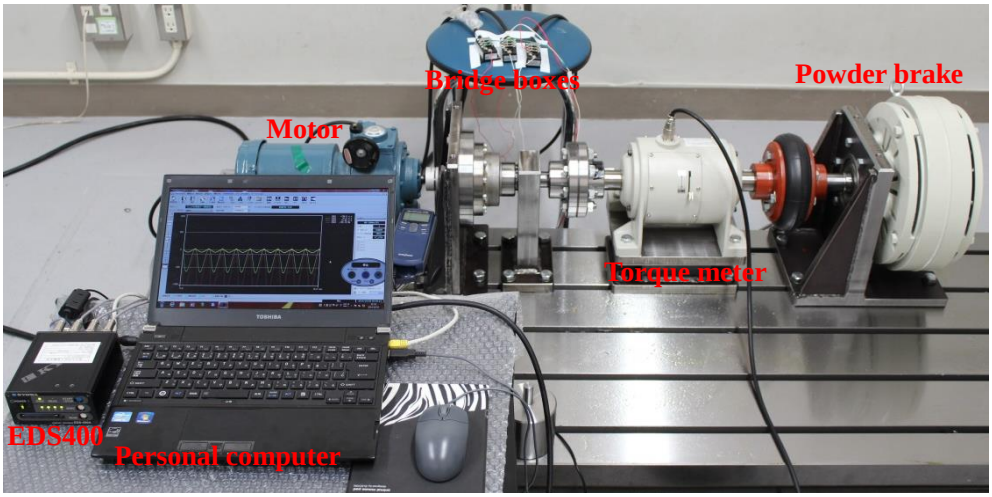

Fig.5 A photo of the experimental device used for the diaphragm strain measurements

4.3 Strain gauge position and directions

A three-directional, strain gauge (gauge length=0.2mm, the smallest size gauge made by Kyowa) is used to measure the diaphragm strains. The strain gauge is stuck on the straight surface of the tapered diaphragm of FS next to the corner of the diaphragm with the boss. This is done before WG is inserted into FS. It means that the strain gauge is stuck before FS, CS and WG are assembled. Then zero point setting (balance adjustment) of the *Wheatstone* bridge circuit is made at this state without assembly. After the zero point setting is finished, WG with FB is inserted into FS and FS, CS and WG are assembled together. Then measurement preparations are completed at this time. Since FS is rotating in the measurements, the strain gauge can be stuck on any position of the circumference direction.

Diaphragm strains are measured under the conditions of zero and 110 Nm torque loads respectively at a very low motor speed about 3 to 5min^{-1}.

Since the corner of the diaphragm with the boss is narrow and sensitive to the strain changes, the corner is not used for the strain measurements. The strain gauge is stuck on the straight part of the tapered diaphragm next to the corner as shown in Fig.6. It is stuck along radial direction, circumference direction and 45-degree direction, a middle position of the radial and circumference directions.

Diaphragm strain signals are sampled by EDS400 when the motor is rotating. The strain signals are changed into digital data directly by EDS400. After the measurements are finished, the personal computer can get the sampled digital strain signals from EDS400.

Normal stresses in the radial and circumference directions and shear stress of the diaphragm at the measurement point are calculated based on the measured strain signals.

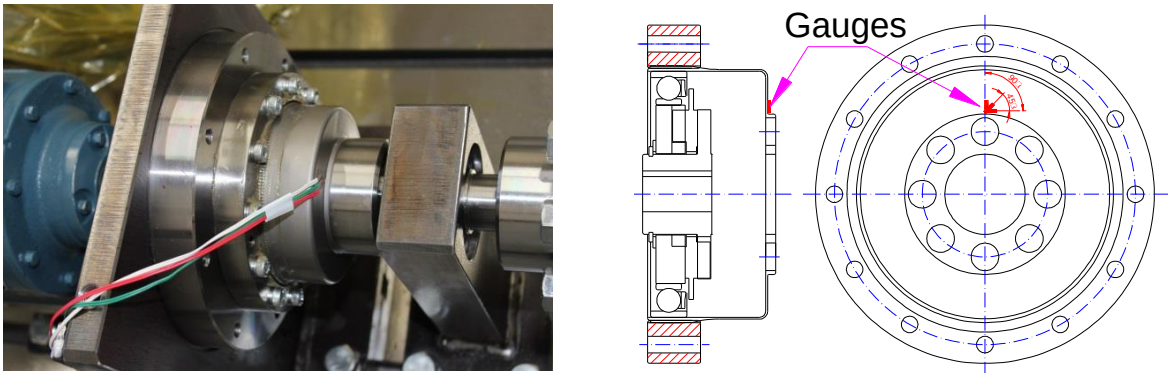

Fig.6 Gage position and directions

4.4 Measurement results and discussions

Figure 7 is the measured strain signals under zero torque. This result is generated only by elliptical deflection of WG. In Fig. 7, the abscissa is sampling time (it also stands for rotational angle of the input shaft of SWG) and the ordinate is the diaphragm strains in the radial direction, the circumference direction and the 45-degree direction respectively. Fig.8 is measured diaphragm strain signals under 110 Nm torque loaded by the powder brake. In Fig. 8, the abscissa and ordinate have the same meanings as in Fig.7.

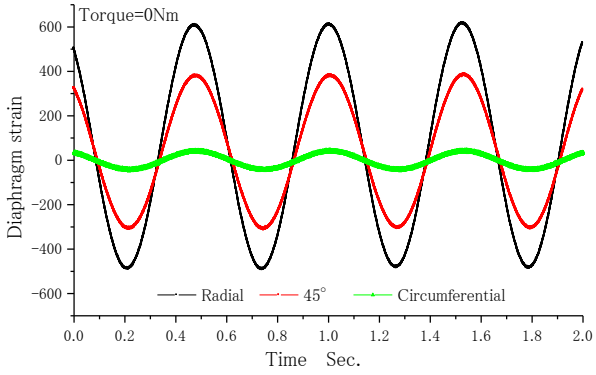

Fig.7 Measured strain signals of the diaphragm under zero torque (Torque=0)

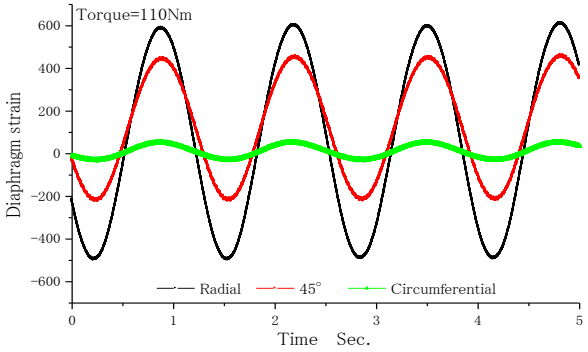

Fig.8 Measured strain signals of the diaphragm under 110Nm torque (Torque =100Nm)

Diaphragm stresses are calculated according to the measured strain signals and given in Figs.9 and 10 respectively. In Figs.9 and 10, the abscissas are sampling time and the ordinates are diaphragm stresses. Fig.9 is the diaphragm stresses under zero torque and Fig.10 is the results under 110 Nm torque.

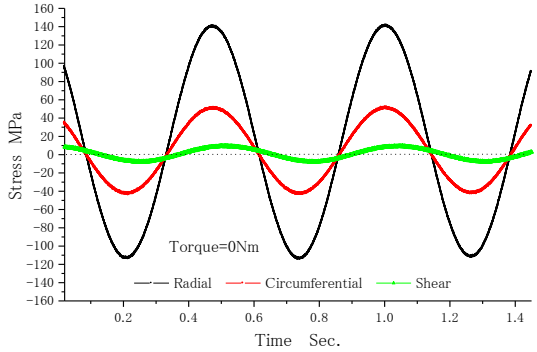

Fig.9 Diaphragm stress signals under zero torque (Torque=0)

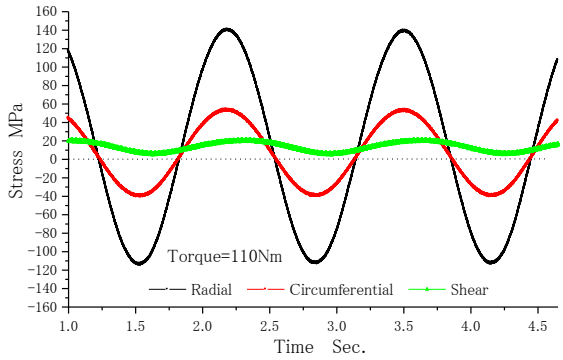

Fig.10 Diaphragm stress signals under 110Nm torque

By comparing Fig.10 with Fig.9, it is found that the normal stresses in the radial and circumference directions almost have no changes when the torque is changed from zero into 110 Nm. The only change is the shear stress. The average value of the shear stress is increased from zero into 13.6MPa when the torque is increased from zero into 110 Nm. Of course, the maximum and minimum values of the shear stress signals are also increased responsively with the increment of the average value. But the amplitude of the shear stress signals almost has no change.

The above phenomenon can be explained like this. The normal stresses in the radial and circumference directions are only resulted from the elliptical deflection of WG (difference between the radius of the major axis and the radius of the minor axis of the elliptical WG). So, if cam shape of WG has no change, the normal stresses in the radial and circumference directions shall keep the same value. The torque has only effect on the average value of the shear stress signals and has nothing to do with the normal stresses in the radial and circumference directions. So, it is reasonable to use the shear stress as an item to evaluate fatigue breakage strength of the diaphragm.

In Fig. 9, it is also found that the shear stress signal takes a shape of sine curve and the average value of the shear stress signal is zero when the torque is zero. This means that the amplitude of the shear stress signal is determined by the elliptical deflection of WG. So, the elliptical deflection of WG also has effect on fatigue breakage strength of the diaphragm.

In Figs. 9 and 10, it is found the normal stresses in radial and circumferential directions are slight asymmetric around horizontal axis. This asymmetry is mainly resulted from the assembly errors of the flex-spline relative to the circular spline. Or say in other words, the axis centerlines of the flex-spline and the circular spline are not coaxial and parallel.

In summary, it can be thought that fatigue breakage of the diaphragm is resulted from the elliptical deflection of WG and the external torque. The amplitude of the shear stress signal of the diaphragm at the corner is determined by the elliptical deflection of WG and the average value of the shear stress signal at the corner is determined by the external torque. So, the average value and amplitude of the shear stress signal at the maximum stress point of the corner can be used as a criterion to evaluate fatigue breakage strength of the diaphragm.

5. Theoretical investigations on the diaphragm stresses

It is quite a difficult thing to conduct stress analysis and strength calculations of SWG in theory. This is because a cup-shaped thin-walled spur gear (the flex-spline) is used in the device and elastic deflection of the thin-walled flex-spline is used to generate tooth engagement movement, a completely different type of tooth engagement movement from usual spur gears. This gearing principle makes the problems of stress analysis and strength calculations of SWG very difficult in theory. Though many researchers attempted to solve the problems in theory and a lot of efforts were made in the past 60 years, the reality is that the problems of stress analysis and strength calculations of SWG have not been solved well since its invention in 1959. Of course, there has been no commercial software available that can do this thing so far.

The author started the research on stress analysis and strength calculations of SWG in 1986 under the advices of Prof. Yunwen Shen, the most famous scholar on harmonic drives in China. From that time on, the author was always thinking to look for a suitable method that can solve the problems of stress analysis and strength calculations of SWG. Finally, the method that is introduced in this paper is formed based on a very long time experiences of the author on FEM and the mathematical programming method. Also, special FEM software is developed responsively by the author through a very long time efforts. As the first step of introductions to the author's research, the method and FEM software are used

to analyze the diaphragm stresses of the flex-spline of SWG at the first. The procedures and calculation results are introduced in the following in detail.

5.1 Basic principle used for contact analysis of SWG

Conry and Serireg [15-16] presented a mathematical programming method used for contact analysis of a pair of elastic bodies in a straight line direction. Ji [18] combined this method with the 2D, FEM in order to be able to conduct loaded tooth contact analysis of a pair of spur gear. Li [19-20] developed Conry and Ji's methods into a three-dimensional (3D), FEM to conduct loaded tooth contact analysis of a thin-rimmed gear with a solid gear using a face-contact model of contact teeth. The mathematical programming method was also developed to solve contact problems of a hypocyclic gear reducer by Li [21].

In this paper, a new model of the mathematical programming method is presented in order to be able to solve contact analysis problem of SWG. In the new model, contact analysis of SWG is conducted along a circumference direction of a pair of gears while the conventional model presented by Conry and Serireg [15-16] only can be used to conduct loaded tooth contact analysis along a straight line direction. This is the main difference of the new model from the conventional one.

Special FEM software is developed to realize contact analysis and stress calculations of SWG through a long time efforts according to the new model. Procedures of the contact analysis and stress calculations of SWG are introduced in the following in detail.

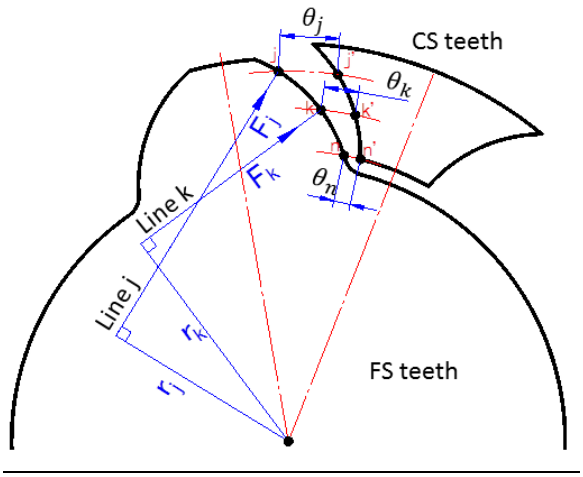

Fig.11 Face-contact model of contact teeth of CS and FS

5.1.1 Deformation Compatibility Relationship

Figure 11 is used to illustrate tooth engagement of an external spur gear (FS) with an internal spur gear (CS) before a torque is applied. It is assumed that only elastic deformation happened in the contact problem of SWG when a torque is applied. Since the tooth engagement of SWG is different from that of usual spur gears in that the former is the tooth engagements on partial surfaces of the tooth profiles from the tip to the root while the latter is the tooth engagements on the geometrical contact lines. So, it is necessary to consider the tooth contacts on the partial surfaces of the tooth profiles from the tip to the root. Or say it briefly, a face-contact model of the contact teeth is necessary for the contact analysis of SWG. This paper presents the face-contact model as stated in the following.

Figure 11 is just an imagining of a pair of teeth that shall come into contact when a torque is applied. Though only one pair of contact teeth is used here to explain the principle of contact analysis developed for SWG, the contact analysis is conducted for all the pairs of contact teeth that have possibility to come into contact when a torque is applied.

In Fig. 11, many pairs of contact points such as (j-j'), (k-k') and (n-n') are made on the tooth surfaces of FS and CS from the tip to the root at the first. These pairs of contact points are made on the same circles at different positions as shown in Fig. 11 and it is assumed that these pairs of contact points have possibility to come into contact when a torque is applied. In Fig.11, j, k and n are the points on the tooth surface of FS and j', k' and n' are the points on the tooth surface of CS. The line j is the common normal line of the pair of contact points (j-j') and the line k is the common normal line of the pair of contact points (k-k'). F_k is contact force between the pair of points (k-k') along their

common normal line. Also, F_j is the contact force between the pair of points (j-j') along their common normal line. Angles (or say backlash) between the pairs (j-j'), (k-k') and (n-n') are denoted as θ_j, θ_k and θ_n respectively. The total angular deformation of FS relative to CS is denoted as φ when CS is fixed and FS is loaded with a torque.

For an optional pair of contact points (k-k'), the angular deformations of the points k and k' can be denoted as φ_k and $\varphi_{k'}$ respectively. If (k-k') comes into contact after a torque is applied, $(\varphi_k + \varphi_{k'} + \theta_k)$, the amount of the angular deformations and the backlash of (k-k'), shall be equal to the total angular deformation φ. But if (k-k') doesn't come into contact, $(\varphi_k + \varphi_{k'} + \theta_k)$ shall be greater than φ. These deformation compatibility relationships can be expressed with two equations of Eq. (1) and (2) in the following. Eq. (1) and (2) can be summarized into Eq. (3).

Eq. (3) is not only suitable for the optional pair of contact points (k-k'), but also suitable for all the pair of contact points made on the tooth surfaces of FS and CS including all the pairs of contact teeth that have possibility to come into contact when SWG is loaded. In Eq. (3), n is the total number of the pairs of contact points.

$$\varphi_k + \varphi_{k'} + \theta_k - \varphi > 0 \quad \text{(Not contact)} \tag{1}$$

$$\varphi_k + \varphi_{k'} + \theta_k - \varphi = 0 \quad \text{(Contact)} \tag{2}$$

$$\varphi_k + \varphi_{k'} + \theta_k - \varphi \geq 0 \quad (k = 1, 2, \dots, n) \tag{3}$$

In Fig.11, if elastic deformations of the points k and k' along the common normal line are denoted as ω_k and $\omega_{k'}$ respectively, ω_k and $\omega_{k'}$ can be expressed with Eq. (4) and (5) when a_{kj} and $a_{k'j'}$ are used. Where, a_{kj} and $a_{k'j'}$ are deformation influence coefficients of the pairs of contact points along their common normal lines. a_{kj} and $a_{k'j'}$ can be obtained by 3D, finite element analysis.

$$\omega_k = \sum_{j=1}^{n} a_{kj} F_j \tag{4}$$

$$\omega_{k'} = \sum_{j=1}^{n} a_{k'j'} F_j \tag{5}$$

As shown in Fig.11, for the optional pair of contact points (k-k'), if ω_k and $\omega_{k'}$ are known, the angular deformation φ_k and $\varphi_{k'}$ can be calculated using Eq. (6). Where, r_k is the distant from the rotational center of FS to the common normal line (the *Line k*) of (k-k').

$$\varphi_k = \omega_k / r_k \;\; ; \quad \varphi_{k'} = \omega_{k'} / r_k \tag{6}$$

If Eq. (4) and (5) are substituted into Eq. (6), then Eq. (7) and (8) can be obtained. If Eq. (7) and (8) are substituted into Eq. (3), then Eq. (9) can be obtained. Also, if Eq. (9) is written into a matrix expression, then Eq. (10) can be obtained.

$$\varphi_k = \sum_{j=1}^{n} a_{kj} F_j / r_k \tag{7}$$

$$\varphi_{k'} = \sum_{j=1}^{n} a_{k'j'} F_j / r_k \tag{8}$$

$$\sum_{j}^{n} \left[\frac{a_{kj} + a_{k'j'}}{r_k} \right] \times F_j + \theta_k - \varphi \geq 0 \quad (k = 1, 2, \dots, n) \tag{9}$$

$$[S]\{F\} + \{\theta\} - \varphi\{e\} \geq \{0\} \tag{10}$$

Where,

$[S] = [S_{kj}] = \left[\frac{a_{kj} + a_{k'j'}}{r_k} \right], k = 1, 2, \dots, n; j = 1, 2, \dots, n$

$\{F\} = \{F_1, F_2, \dots, F_k, \dots, F_n\}^T$
$\{\theta\} = \{\theta_1, \theta_2, \dots, \theta_k, \dots, \theta_n\}^T$
$\{e\} = \{1, 1, \dots, 1\}^T$
$\{0\} = \{0, 0, \dots, 0\}^T$

5.1.2 Force Equilibrium Relationship

Except for the deformation compatibility relationship as shown in Eq. (10), a force equilibrium relationship can also be built as given in Eq. (11). Where, T is the external torque applied on FS.

$$\sum_{k=1}^{n} r_k \times F_k = T \qquad (k = 1, 2, \dots, n) \qquad (11)$$

If Eq. (11) is written into a matrix form, Eq. (12) can be obtained. Where, $\{r\} = \{r_1, r_2, \dots, r_k, \dots, r_n\}$

$$\{r\}^T\{F\} = T \qquad (12)$$

Eq. (10) and (12) can be used as constrain conditions to identify which pair of contact points is in contact and which pair is not in contact. Then, the contact problem of SWG can be explained as looking for the contact force F_j $(j = 1,2,3, \dots, n)$ between the pairs of contact points that must satisfy Eq. (10) and (12) under the conditions of knowing the deformation influence coefficients a_{kj}, $a_{k'j'}$, the backlash angle θ_k, the radius r_k and the external torque T in advance.

5.1.3 A Model of the Mathematical Programming Method Used for Contact Analysis of SWG

A model of the mathematical programming method can be made to solve the contact problem of SWG as follows. Since Eq. (10) is an inequality constraint equation that may be strictly positive or identically zero, it can be transformed into an equality constraint equation by introducing a so-called slack variable $\{Y\}$ (consists of positive variables) based on the principle of Modified Simplex Method. Then Eq. (13) and (14) can be obtained.

$$[S]\{F\} + \{\theta\} - \varphi\{e\} - [I]\{Y\} = \{0\} \qquad (13)$$

or

$$-[S]\{F\} + \varphi\{e\} + [I]\{Y\} = \{\theta\} \qquad (14)$$

Where
$\{Y\} = \{Y_1, Y_2, \dots, Y_k, \dots, Y_n\}^T$ (Slack variables)
$[I]$= a unit matrix of n×n

Then two equality constraint equations of Eq. (12) and (14) are obtained. The next thing is to make an objective function Z that is necessary for the model of the mathematical programming method. The objective function Z can be made through introducing some positive variables X_{n+1}, X_{n+2}, ..., X_{n+n}, X_{n+n+1} (usually called artificial variables) to every constrain equation based on the principle of Modified Simplex Method. Then the model of the mathematical programming method used for the contact analysis of SWG can be made as follows.

The Model of Mathematical Programming Method:
Objective Function:
$Z = X_{n+1} + X_{n+2} + \cdots + X_{n+n} + X_{n+n+1}$ (15)
Constraint Conditions:
$-[S]\{F\} + \varphi\{e\} + [I]\{Y\} + [I]\{Z'\} = \{\theta\}$ (16)
$\{r\}^T\{F\} + X_{n+n+1} = T$ (17)
Where,
$[S] = \left[S_{kj}\right] = \left[\frac{a_{kj} + a_{k'j'}}{r_k}\right], k = 1, 2, \dots, n; j = 1, 2, \dots, n$
$\{Z'\} = \{X_{n+1}, X_{n+2}, \dots, X_{n+n}\}^T$ (artificial variables)
$\{F\} = \{F_1, F_2, \dots, F_k, \dots, F_n\}^T$
$\{Y\} = \{Y_1, Y_2, \dots, Y_k, \dots, Y_n\}^T$ (slack variable)

$\{\theta\} = \{\theta_1, \theta_2, \dots, \theta_k, \dots, \theta_n\}^T$
$\{r\} = \{r_1, r_2, \dots, r_k, \dots, r_n\}^T$
$\{e\} = \{1, 1, \dots, 1\}^T$
$F_k \geq 0, Y_k \geq 0, \theta_k \geq 0, \theta \geq 0, k = 1, 2, \dots, n$
$X_{n+m} \geq 0, m = 1, 2, \dots, n+1$

The contact force F_k and the total angular deformation φ can be calculated by minimizing the objective function Z under the constrain conditions of Eq. (16) and (17).

5.2 Software development

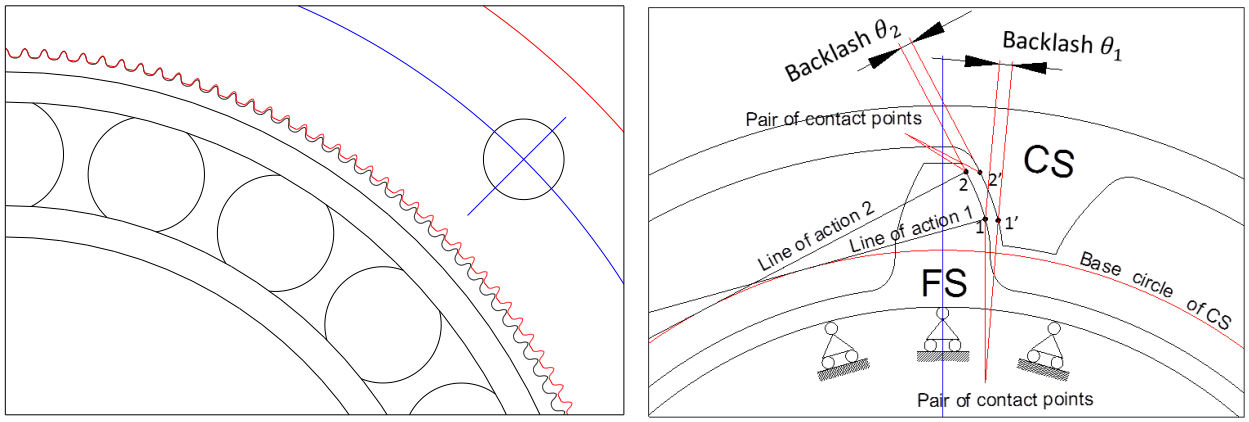

(a) Section view of SWG (b) Section view of mechanics model

Fig.12 Section structure and Mechanics model used for loaded gear contact analysis

In Fig.12, (a) is a section view of SWG when CS, FS and WG with FB are assembled together and (b) is a section view of 3D, mechanics model used for the contact analysis of SWG. As shown in Fig.12 (b), in order to simplify the procedures of contact analysis between FS and WG with FB, outer ring of FB is neglected in the analysis and the contact between FS and WG is simplified into the contact between the inner surface of FS and balls of FB. At the first, all balls (23 balls) are used to support FS. When FEM is used to conduct the contact analysis, the supports of 23 balls are replaced by the supports of 23 boundary nodes as shown in Fig.12 (b). These boundary nodes can only support FS along the radial directions at their contact positions and are free in axial and circumferential directions.

Contact states of the balls are identified according to the reaction forces (supporting loads) on the boundary nodes. If the reaction force on a boundary node is a compressive load, this means that this ball is working and the boundary node should be used continually to support FS. Otherwise, if the reaction force on a boundary node is a tensile load, this means that this ball is not working and the boundary node should be removed from the support conditions in the next one calculation. This identification is made for all the balls (all the boundary nodes) and repeated until contact states of all the balls are not changed again.

As it is mentioned above, a lot of pairs of contact points are made on tooth surfaces of FS and CS before the contact analysis is conducted and it is assumed that all the pairs of contact points have possibility to come into contact when a torque is applied. Also, a lot of pairs of contact teeth like the pair of teeth shown in Fig. 12(b) are made and used for the contact analysis of SWG and it is assumed that all the pairs of contact teeth have possibility to come into contact when the torque is applied. Finally, judgments are made for all the pairs of contact teeth and all the pairs of contact points as follows through the contact analysis using developed FEM software.

If the calculated contact force between a pair of contact points is zero, it means that this pair of contact points is not in contact. Otherwise, it means that this pair of contact points is in contact. The similar judgment is made for pairs of contact teeth. If the contact forces on a pair of contact teeth are zero, it means that this pair of contact teeth is not in contact. Otherwise, it means this pair of contact teeth is in contact. The procedures of the contact analysis are stated as follows using two pairs of contact points shown in Fig. 12(b) as an example.

In Fig. 12(b), two pairs of contact points (1-1') and (2-2') are made on tooth surfaces of FS and CS. It is assumed that they have possibility to be in contact when a torque is applied. The lines of action of (1-1') and (2-2') are illustrated as "Line of action 1" and "Line of action 2" in Fig.12 (b) respectively. These lines of action are also the common normal lines of the pairs of contact points. Contact forces are along the lines of action. When involute curves are used as tooth profiles of FS and CS, these lines shall be tangential to the same base circle of CS at different places as shown in Fig. 12(b). But if the tooth profiles of FS and CS are not involute curves, these lines shall be tangent to different circles with

different radiuses like the case as shown in Fig.11. The main procedures used for FEM software development are introduced in the following.

Procedures of FEM software development:

Step 1: Choose a range of the pairs of contact teeth used for contact analysis through determining a total number of the pairs of contact teeth used for contact analysis.

Step 2: Make a lot of pairs of contact points on tooth surfaces of FS and CS for all the pairs of contact teeth used.

Step 3: Calculate backlashes and r_k of all the pairs of contact points for all the pairs of contact teeth according to the coordinates of the contact points.

Step 4: Calculate deflection influence coefficients of all the pairs of contact points with 3D, FEM by applying a unit force along the common normal lines and calculating deformations of the contact points in the directions of the common normal lines. At this time, FS is supported by bearing balls and the boss of FS is fixed as the boundary conditions of FEM calculations for FS. Also, outside cylindrical surface of CS is fixed as the boundary conditions of FEM calculations for CS at this time.

Step 5: Substitute torque load, deflection influence coefficients of FS and CS, backlashes and r_k of all the pairs of contact points into Eq. (16) and (17) to calculate contact force F_k and the total angular deformation φ through solving Eq. (15), (16) and (17) using the Modified Simplex Method.

Step 6: Calculate reaction forces on the balls according to tooth loads obtained in Step 5 and identify contact states of all the balls according to directions of the reaction forces on the balls. Determine a new support condition of the balls based on the contact states of the balls for the next cycle of calculations. If there is no more change in the contact states of the balls between the last cycle of contact analysis and this cycle of contact analysis, then go to Step 7. Otherwise go to Step 4 and repeat the procedures (cycle) from Step 4 to Step 6.

Step 7: Calculate diaphragm stresses of FS using FEM under the conditions that the contact forces are applied on the tooth surfaces of FS, the inner surface of FS is supported by balls and the boss is fixed.

Step 8: End of the analysis.

5.3 FEM mesh-dividing patterns

Figure 13 is 3D, FEM model and mesh-dividing patterns used for contact analysis and stress calculations of CSF40-100. In Fig.13, (a) is a 3D view of the FEM model from the open end of FS, (b) is a 3D view of the FEM model from the real of FS and (c) is an enlarged view of contact teeth. As it is well-known, FS and CS teeth are engaged in two areas (two sides of the major axis of WG, or the upper and lower parts in Fig. 13). Since the teeth at the two areas are in the same engagement states in theory (machining and assembly errors are neglected), it is only necessary to consider the tooth contacts at one area (the upper part of the teeth is used in Fig. 13) if the mathematical programming method is used for contact analysis. This is the advantage of the mathematical programming method used for contact analysis that contact analysis of contact teeth with the same contact states can be omitted.

Figure 14 is enlarged section views of mesh-dividing patterns of FS and CS teeth. In Fig.14, (a) is the case that FS is not deformed by WG (WG is not assembled) and (b) is the case that FS is deformed by WG (FS, CS and WG with FB are assembled together).

Super-parametric hexahedron solid element, which has 8 nodes at the corner and 3 nodes inside the element, is used in FEM programming. The detailed introduction about this element can be found in the reference [22].

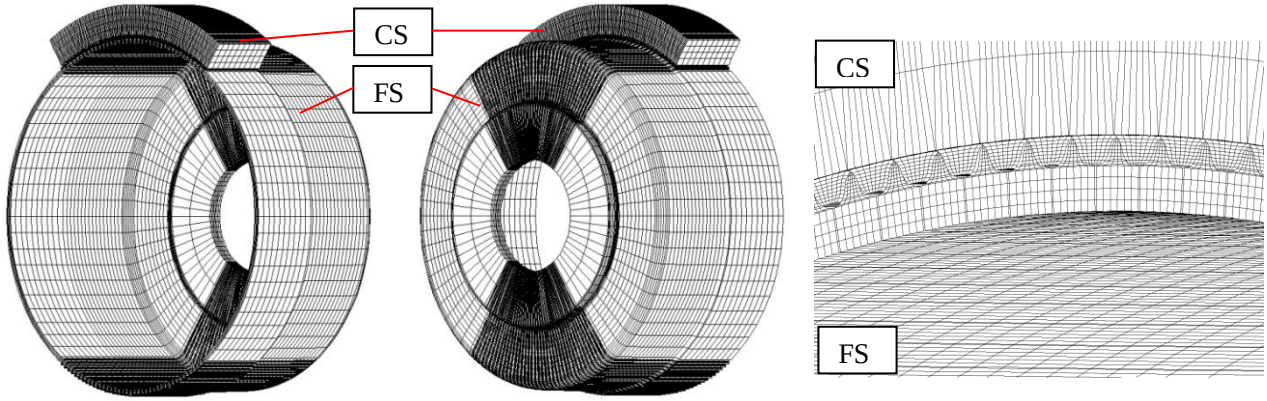

(a) Open end of FS and CS (b) Real of FS and CS (c) Enlarged view of contact teeth

Fig.13 3D, view of FEM mesh-dividing of CS and FS

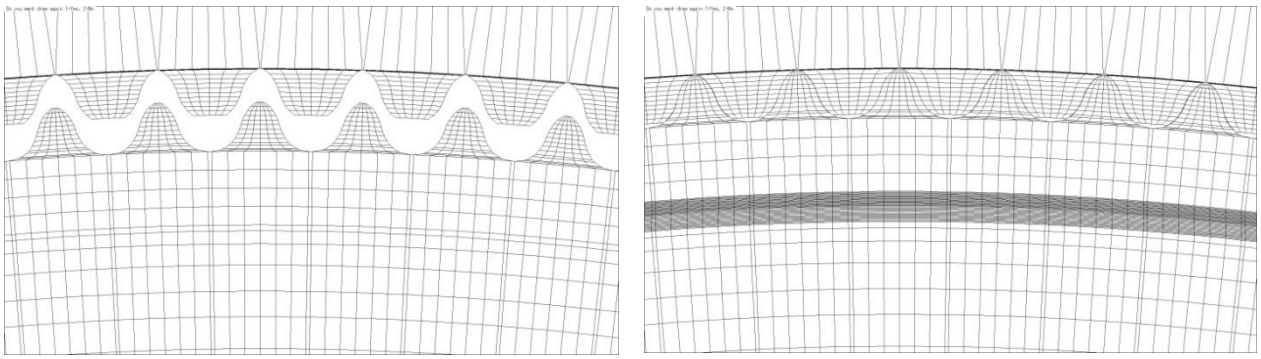

(a) CS and FS before WG is assembled (b) CS and FS after the WG is assembled

Fig.14 Enlarged section-view of mesh-dividing patterns of CS and FS teeth

5.4 Calculated diaphragm stresses and comparisons with the measured ones

Figure 15 and 16 are calculated diaphragm stresses at the same point of the strain measurements. Fig. 15 is the result under zero torque and Fig.16 is the one under 110 Nm torque. In Figs.15 and 16, the abscissas are angles used to stand for circumferential positions of the calculation point when FS is rotated one revolution. The ordinates are diaphragm stresses calculated by developed FEM software.

By Comparing the calculated results shown in Figs.15 and 16 with the measured ones shown in Figs.9 and 10 respectively, it is the found that the calculate results are in agreement with the measured ones well. This means that the model, method and FEM software presented in this paper are correct and effective for diaphragm stress analyses and strength calculation of SWG.

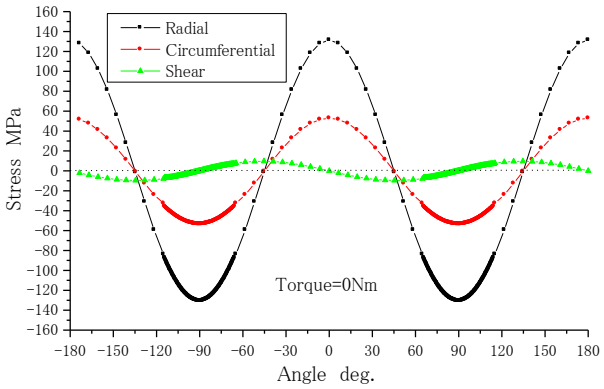

Fig.15 Calculated diaphragm stresses under zero torque (Torque=0)

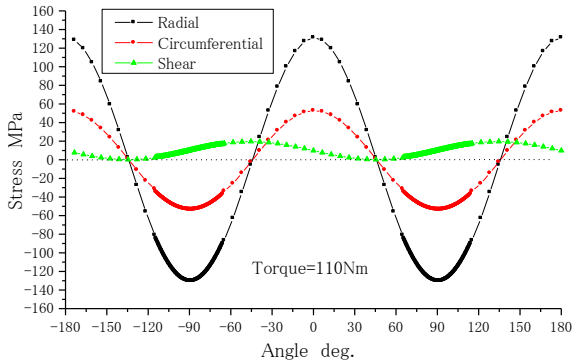

Fig.16 Calculated diaphragm stresses under 110Nm torque (Torque=110Nm)

5.5 Diaphragm stresses of the maximum stress point

It is found that the maximum stress point at the corner of the diaphragm with the boss is located near the middle point of the corner (not exact at the middle point) based on results of FEM analyses. This position is in agreement with the position of diaphragm fatigue breakage very well. Diaphragm stresses of the maximum stress point are investigated with the developed FEM software. Calculation results are introduced in the following.

Figure 17 is the radial stresses of the maximum stress point. It is calculated under four torque conditions: torque=0, 75, 121 and 171Nm respectively. In Fig. 17, the abscissa is an angle used to stand for circumferential position of the maximum stress point and the ordinate is the radial stresses calculated. Figure 17 indicates that the external torque has no effect on the radial stresses. This means that the radial stresses of the maximum stress point are only resulted from the elliptical deflection of WG.

Figure 18 is the circumferential stresses of the maximum stress point. In Fig. 18, the abscissa is an angle used to stand for circumferential position of the maximum stress point and the ordinate is the circumferential stresses calculated. Figure 18 also indicates that the external torque has no effect on the circumferential stresses. The circumferential stresses of the maximum stress point are determined only by the elliptical deflection of WG.

Figure 19 is the shear stresses of the maximum stress point. In Fig. 19, the abscissa is an angle used to stand for circumferential position of the maximum stress point and the ordinate is the shear stresses calculated. In Fig.19, it is found that amplitude of the shear stress waveform has no changes when the external torque is increased, but the average value of the shear stress waveform is increased with the increment of the torque. A relationship between the external torque and the average value of the shear stress waveform is given in Fig. 20. In Fig.20, it is found that the average value of the shear stress waveform is a linear relation with the torque. This means that the amplitude of shear stress waveform is determined by the elliptical deflection of WG, but the average value of shear stress waveform is resulted from the torque.

Since the experimental and theoretical results obtained in this paper show that the external torque has effect only on the shear stress of the maximum stress point at the corner of the diaphragm with the boss, it is suggested in this paper that the fatigue breakage strength of the diaphragm should be evaluated using the amplitude and average value of the shear stress waveform of the maximum stress point. Goodman diagram can be used to do the evaluation. Figure 21 is a concept of using the amplitude and the average value of the shear stress waveform in Goodman diagram for fatigue strength evaluation of the diaphragm.

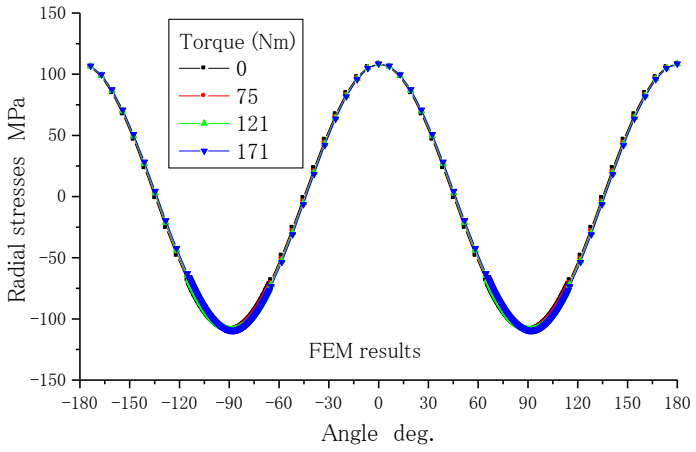

Fig.17 Effect of the external torque on radial stress of diaphragm

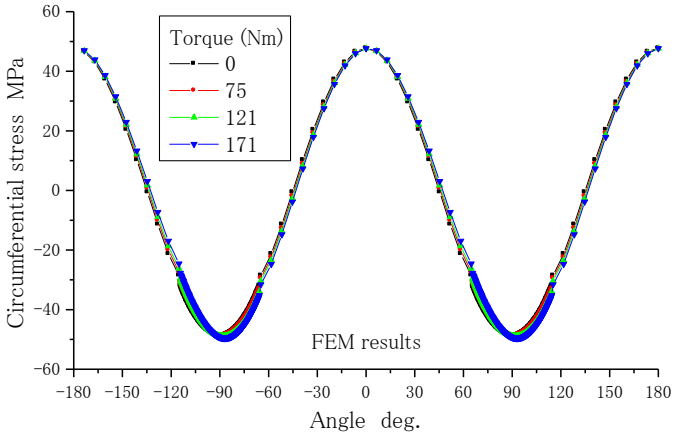

Fig.18 Effect of the external torque on circumferential stress of diaphragm

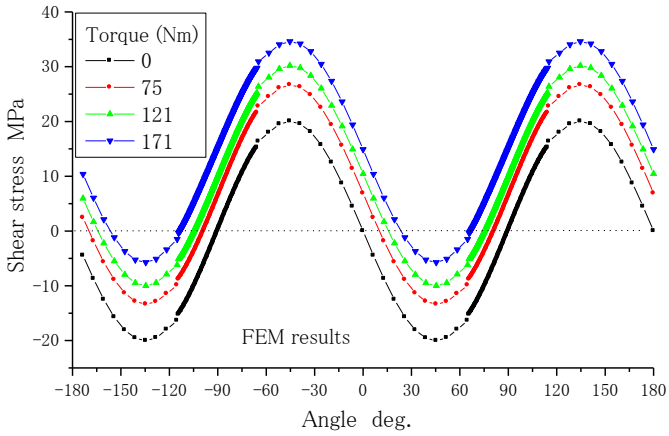

Fig.19 Effect of the external torque on shear stress of diaphragm

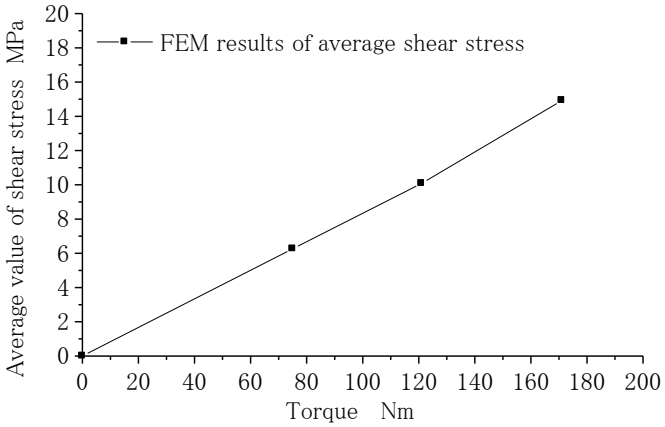

Fig.20 Effect of the external torque on shear stress of diaphragm

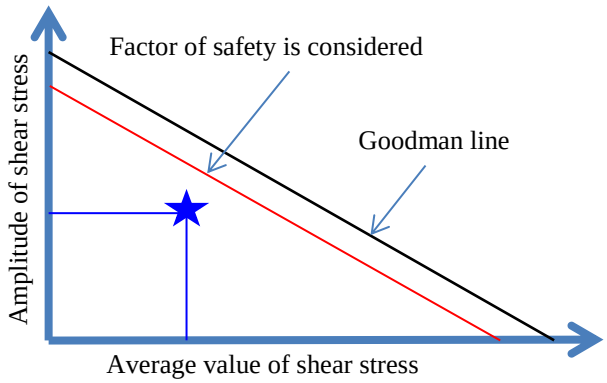

Fig.21 Fatigue strength evaluation method presented for the diaphragm

6. Conclusions

1) An experimental method and apparatus are presented in this paper to measure diaphragm strains of the flex-spline, a thin-walled spur gear used in the strain wave gearing. Diaphragm stresses next to the corner of the diaphragm with the boss are investigated experimentally.
2) Three-dimensional, mechanics model and finite element method are presented in this paper to conduct contact analysis and stress calculations of the strain wave gearing in theory through a very long time efforts. Special FEM software is developed for the strain wave gearing based on the model and method presented in the paper.
3) Diaphragm stresses of the measurement point obtained by the FEM software are in agreement well with the ones calculated using the measured strains. This means that the presented methods and developed software are correct and effective for diaphragm stress analysis and fatigue strength calculation of the flex-spline.
4) Shear stress of the maximum stress point at the corner is the reason to result in diaphragm fatigue breakage. It is suggested using the amplitude and the average value of the shear stress waveform at the maximum stress point as the criterion to evaluate fatigue strength of the diaphragm breakage at the corner.

References

1) C. W. Musser, Strain wave gearing, Unite States Patent, No.2906143, 1959.
2) C. W. Musser, Breakthrough in mechanical drive design-The harmonic drive, Machine Design April (1960) 160-173.
3) Y. Shen, Q. Ye, Design theory and design methods of a harmonic drive transmission, China Machine Press, Beijing, China, 1985.
4) M. H. NBAHOB (translated by Y. Shen, K. Li), Harmonic drive transmission, National Defense Industry Press, Beijing, China, 1987.
5) N.A. Alfutov, S.S. Klenikov, Calculation of forces of interaction of harmonic drive elastic elements by a step-by-step method, Russian Engineering Journal 58(7) (1978) 26-29.
6) K. Le, Y. Shen, Analysis method of bearing loads distributed on wave generator of a harmonic drive device, Mechanical Science and Technology for Aerospace Engineering 34(2) (1990) 38-45.
7) K. Le, Study on tooth load distribution and optimal tooth modifications of a harmonic drive device, thesis of master degree Northwestern Polytechnical University, China, 1988.
8) B. Chui, Tooth contact load and contact stress analyses of a harmonic drive gearing, thesis of master degree Northwestern Polytechnical University, China, 1994.
9) T. Ishida, T. Ohshita, Y. Kiyosawa, X. Zhang, A method for measuring load on bearing balls in strain wave gearing, Trans. Jpn. Soc. Mech. Eng. 64(626) (1998) 4003-4008 (Sec. C).
10) H. Sentoku, T. Satou, Y. Kiyosawa, X. Zhang, Characteristics of load transmission in strain wave gearing (1st Report, Derivation of load distribution on tooth flank), Trans. Jpn. Soc. Mech. Eng. 70 (696) (2004) 2515-2522 (Sec. C).
11) B. Routh, R. Maiti, A.K. Ray and A. Sobczyk, An investigation on secondary force contacts of tooth pairs in conventional harmonic drives with involute toothed gear set, Proceedings of the Institution of Mechanical Engineers, Part C: Journal of Mechanical Engineering Science 230(4) (2015) 622-638.
12) V. Sahoo and R. Maiti, Static load sharing by tooth pairs in contact in internal involute spur gearing with thin

rimmed pinion, Proceedings of the Institution of Mechanical Engineers, Part C: Journal of Mechanical Engineering Science 230(4) (2016) 485-499.
13) S. Li, Y. Shen, Fatigue failure patterns and strength design methods of a harmonic drive device, The 11th World Congress in Mechanism and Machine Science, Tianjin, 2004, pp.805-810.
14) S. Li, Fatigue failure patterns and strength design methods of a three-dimensional, extremely thin-walled spur gear, The JSME Symposium on Motion and Power Transmissions, Osaka, 2004, pp.128-129.
15) T.F. Conry, A. Serireg, A mathematical programming method for design of elastic bodies in contact, Trans. ASME, J. Appl. Mech. 6 (1971) 387-392.
16) T.F. Conry, A. Serireg, A mathematical programming method for evaluation of load distribution and optimal modifications for gear system, Trans. ASME, J. Eng. Ind. 11(1973) 1115-1122.
17) Product catalog of Harmonic Drive Systems Inc.
18) M. Ji, A method for contact analysis of elastic bodies using FEM and a mathematical programming method, research report of Northwestern Polytechnical University, China, No.SHJ8032 (1980) 1-18.
19) T. Ishida, S. Li, A method for analyzing tooth load distribution and contact stress of a thin wall spur gear using FEM and a mathematical programming method, Trans. Jpn. Soc. Mech. Eng. 63(606) (1997) 585-591 (Sec. C).
20) S. Li, Gear contact model and loaded tooth contact analysis of a three-dimensional, thin-rimmed gear, Trans. ASME, J. Mech. Des. 124(3) (2002) 511-517.
21) S. Li, Contact problem and numeric method of a planetary drive with small teeth number difference, Mech. Mach. Theory 43(9) (2008) 1065-1086.
22) G. Liu, Structural Dynamics of the Finite Element Method (In Chinese), National Defense Industry Press, Beijing, China, 1994.